International Journal on Theoretical and Applied Research in Mechanical Engineering

ISSN: 2319-3182

Volume 12 Issue 1 (2023) | Pages: 33-47

Experimental Analysis of Forced Convective Drying of Coriander

Roshan Morde[1], Bharat Thorat[2], Hrishikesh Perke[3], Sammed Patil[4], Sagar Chirade[5*]

[1,2,3,4,5]Department of Mechanical Engineering, Indira College of Engineering and Management, Parandwadi, Pune, 410506, Maharashtra, India

*Corresponding Author: chiradesagar@gmail.com

Peer Review Information

Type: *Article*
Received: *03 May 2023*
Revised: *27 May 2023*
Accepted: *22 June 2023*
Published: *26 July 2023*

Abstract

A convection hot air dryer utilizes forced thermal convection to accelerate moisture evaporation from perishable agricultural produce. This study presents a comprehensive experimental investigation and Computational Fluid Dynamics analysis of the forced convective hot air drying characteristics of coriander. The experimental apparatus integrates a wooden drying chamber, an electric heating unit, a centrifugal blower, and a digital mass sensor. Drying performance was systematically evaluated across multiple air inlet velocities at a controlled drying air temperature for different sample batch masses. Three-dimensional steady-state fluid dynamics simulations executed via ANSYS Fluent resolved the internal aerodynamic streamlines, velocity field distributions, and wall pressure contours. Numerical findings revealed stagnation zones within specific regions of the drying chamber where air circulation is severely restricted, while highlighting high-impact stress regions along the wall directly opposing the inlet duct. Experimental mass-loss kinetics demonstrated that elevated air velocities significantly reduce drying time requirements. The integration of computational visualization confirmed that positioning drying trays in parallel alignment with the principal airflow vectors significantly enhances thermal performance and moisture removal kinetics.

Keywords: Forced Convective Drying; Coriander Preservation; Computational Fluid Dynamics; ANSYS Fluent; Drying Kinetics; Heat and Mass Transfer.

How to Cite This Article

Morde, R., Thorat, B., Perke, H., Patil, S., & Chirade, S. (2023). Experimental analysis of forced convective drying of coriander. *International Journal on Theoretical and Applied Research in Mechanical Engineering, 12*(1), 33–47.

Introduction

Convective hot air dryers remove moisture from organic or industrial materials through forced thermal convection, accelerating moisture evaporation and stabilization. In modern industrial processing, forced convective drying is extensively utilized across food processing, pharmaceuticals, and chemical manufacturing. The fundamental architecture of a convective hot air drying unit incorporates an electric or thermal heating element, a centrifugal blower to enforce directional circulation, and an insulated drying chamber holding the target substrate. The heated air stream passes over or through the substrate, establishing a vapor pressure differential that drives internal moisture toward the boundary layer, where it is absorbed and expelled to the external environment.

Coriander is an essential aromatic herb widely cultivated for culinary and medicinal applications due to its distinct essential oils and bioactive compounds. However, fresh coriander possesses high initial moisture content and high natural perishability, leading to rapid post-harvest degradation. Effective post-harvest dehydration is required to inhibit microbial activity, prevent enzymatic spoilage, and extend shelf life while maintaining essential nutritional, aroma, and color attributes. Controlled convective hot air drying reduces moisture content efficiently, facilitating long-term storage and transportation.

This investigation combines empirical thermal testing with Computational Fluid Dynamics using ANSYS Fluent to model the internal transport processes. The numerical framework evaluates three-dimensional velocity streamlines, wall pressure contours, and recirculation patterns to identify structural stagnation zones and optimize internal chamber aerodynamics. Convective hot air drying supports modern agricultural value chains, including snack manufacturing, bulk weight reduction, year-round product availability, compact storage, and raw ingredient preparation for ready-to-eat formulations.

Literature Review

Understanding convective thermal drying requires reviewing established drying models, transport kinetics, and quality characteristics across various agricultural products. Table 1 summarizes key literature parameters, sample geometries, and experimental drying conditions.

Table 1. *Summary Of Literature on Convective Drying Parameters And Methodologies*

Sample Material	Sample Thickness	Temperature	Velocity	Methodology / Equipment Type
Spinach	Millimeter range	Moderate to high	Standard forced flow	Pilot-scale cabinet convective dryer
Coriander	Millimeter range	Moderate to high	Standard forced flow	Fixed bed dryer
Moringa	Millimeter range	Moderate to high	Low velocity flow	Convective type dryer
Lettuce	Millimeter range	Moderate	Standard forced flow	Indirect solar dryer
Apricots	High thickness	High thermal input	High air speed	Air flow velocity system
Potato	Sliced geometry	Low to high	High air speed	Air flow velocity system
Banana	Sliced geometry	Low to high	Low velocity flow	Air flow velocity system
Carrot	Sliced geometry	Moderate	Low velocity flow	Air flow velocity system
Onion	Sliced geometry	Low to moderate	Moderate air speed	Moderate air velocity unit
Apple	Sliced geometry	High thermal input	Moderate air speed	Hot air drying system
Pomegranate	Thin layer	Low to high	Standard forced flow	Kinetic drying method
Cucumber	Sliced geometry	Low to moderate	Moderate air speed	Kinetic drying method

Raisin	Thin layer	Low to moderate	Moderate air speed	Convective drying method
Watermelon	Sliced geometry	Low to moderate	Moderate air speed	Kinetic drying method
Pumpkin	Sliced geometry	Moderate	Standard forced flow	Hot air drying system
Guava	Sliced geometry	Moderate	Low velocity flow	Hot air drying system
Garlic	Sliced geometry	Low to moderate	Low velocity flow	Air flow velocity system
Ginger	Sliced geometry	High thermal input	High air speed	Hot air drying system
Chili	Thin layer	Moderate	Low velocity flow	Preliminary drying procedure
Radish	Sliced geometry	High thermal input	High air speed	Convective drying method
Chana	Granular geometry	Moderate to high	Moderate air speed	Convective drying method
Green Peas	Granular geometry	Moderate to high	High air speed	Convective drying method

Usama evaluated the effect of sequentially reducing temperature profiles during convective potato slice drying. Stepwise temperature reduction preserved original color attributes with an increase in overall drying time relative to constant high-temperature dehydration. Kilic analyzed hot air drying kinetics for carrots, zucchini, and eggplants across varying thermal conditions. Drying occurred entirely within the falling rate period, and raising temperatures resulted in a systematic reduction of total drying times across all species. Thin-layer mathematical modeling yielded strong correlations, identifying distinct theoretical models suitable for carrot, zucchini, and eggplant kinetics.

Ionut examined apple and apricot dehydration in a pilot system across varied air speeds and thermal conditions. Higher velocities and thermal inputs accelerated moisture loss and solid gain while causing volumetric shrinkage and ascorbic acid degradation. Zeng investigated hybrid infrared and hot air drying of carrot slices using Response Surface Methodology. Variations in processing conditions directly impacted moisture diffusivity, specific energy consumption, volumetric shrinkage, rehydration ratios, and total color change.

Pilot-scale convective drying of blackberries showed that non-linear mathematical models provided superior experimental agreement. Thin-layer tomato slice drying demonstrated that effective moisture diffusivity increases as processing temperature rises. Convective tray drying of apple slices confirmed that empirical regression models effectively capture thin-layer moisture removal behavior. Studies on oyster mushrooms also established high predictive accuracy when fitting experimental data to standard convective drying models.

Research Gap

While convective drying characteristics have been documented for root vegetables, fleshy fruits, and robust commodities, detailed theoretical and numerical studies on high-surface-area leafy herbs like coriander remain limited. Prior research primarily reports global bulk mass loss without mapping local fluid dynamics or internal aerodynamic dead zones within the enclosure. Combining physical drying experiments with three-dimensional fluid dynamics flow visualizations helps resolve how localized internal velocity fields directly influence herb drying kinetics.

Novelty

This work integrates full three-dimensional numerical aerodynamic flow analysis with physical experiments in a custom-built forced-convective drying apparatus. It identifies structural aerodynamic stagnation zones, maps wall pressure boundaries, and links localized internal flow profiles directly to real-time coriander mass-loss rates across multiple inlet velocities and batch loads.

Objectives

1. Conduct aerodynamic flow field simulations within a box-type convective hot air dryer using ANSYS Fluent.
2. Evaluate thermal and velocity distribution profiles inside the drying enclosure.

3. Analyze the impact of air inlet velocity, process duration, and temperature on coriander moisture loss.
4. Quantify drying time and thermal energy requirements during herbal dehydration.
5. Complete structural design, CAD modeling, component integration, and experimental validation of the physical dryer.

Materials and Methods

Fresh coriander was harvested, washed, and sorted to remove surface impurities and residual dirt. Sorted samples were weighed into distinct batch masses and spread evenly across drying trays. Experimental runs were conducted at controlled operating temperatures across multiple air velocities. Mass reduction was monitored at regular time intervals using a digital balance integrated into the drying assembly. Inlet and outlet dry-bulb temperatures, relative humidity, and air speeds were logged continuously using calibrated thermocouple arrays, hygrometers, and a digital vane anemometer.

Design Methodology

The experimental apparatus was designed to establish optimal positioning for the centrifugal air blower, inline heating unit, connecting ductwork, and primary drying chamber. The design features an inline configuration where air is pressurized by the blower, passed over resistance heating elements, and introduced laterally into the lower section of the drying box. Outlet exhausts located at the top surface allow humid air to escape continuously. The digital mass balance is isolated on the upper frame to record sample weight in real time during testing.

Mathematical Modelling

Convective thermal transfer from hot air to the target substrate surface is theoretically governed by Newton's Law of Cooling, which establishes that heat flux is directly proportional to the surface area and the temperature differential between the solid substrate and the bulk fluid stream. Thermal transport through solid boundaries and static bed layers is described by Fourier's Law of Heat Conduction, where thermal energy transfer depends on the intrinsic thermal conductivity of the material and the spatial temperature gradient. Forced convective heat transfer coefficients are theoretically evaluated using dimensionless Nusselt number correlations, which express heat transfer efficiency as a function of fluid momentum, represented by the Reynolds number, and fluid thermal diffusion properties, represented by the Prandtl number.

Governing Equations

Fluid movement and thermal energy transport within the drying chamber are governed by the classical continuum mechanics conservation laws formulated in three-dimensional Cartesian coordinates.

Mass conservation dictates that the temporal rate of change of fluid density within a control volume must balance the net spatial flux of fluid mass crossing its boundary surfaces. Momentum transport is dictated by the Navier-Stokes equations, which express Newton's second law for fluid continua, balancing local fluid acceleration against pressure gradient forces, viscous shear stress tensors, and gravitational body forces. Energy transport is governed by the first law of thermodynamics, maintaining that temporal changes in total fluid energy are equal to net conductive and convective thermal transport, work performed by viscous pressure forces, and internal volumetric thermal generation.

Experimental Setup

The experimental assembly, designed conceptually as shown in Fig. 8 and constructed physically as shown in Fig. 9, consists of the following integrated systems:

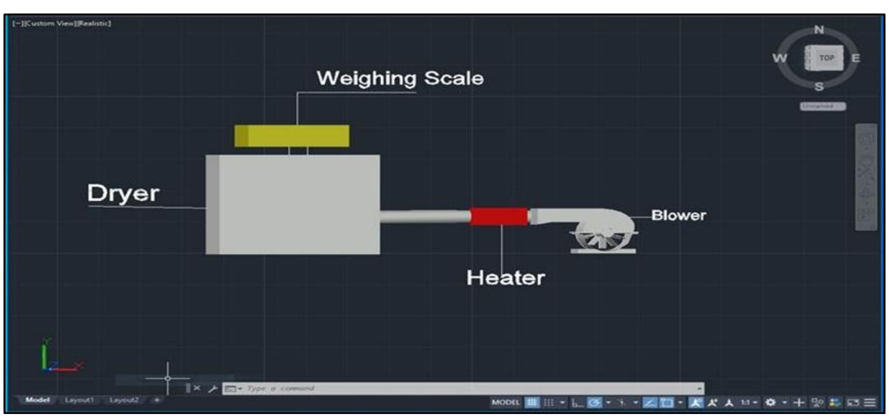

Fig. 8. *Schematic layout detailing the convective hot air dryer assembly, blower unit, inline heater, connecting ducting, and weighing balance.*

Fig. 9. *Fully operational physical experimental setup showing the centrifugal blower, heating ductwork, insulated wooden drying chamber, instrumentation, and control unit.*

- Centrifugal Blower Unit: Operates to supply controlled volumetric airflow through the ducting assembly into the drying enclosure.
- Electric Heating System: An inline electric heating assembly that raises incoming ambient air to the target process drying temperature.
- Insulated Wooden Drying Chamber: Formed from thick structural timber to minimize thermal loss and maintain uniform interior processing conditions.
- Digital Weighing Scale: Positioned on the upper external frame to continuously monitor batch mass loss without disturbing internal airflow.
- Vane Anemometer: Measures incoming and internal air velocity profiles.
- Thermocouples and Hygrometers: Strategic sensor arrays installed at the inlet duct, internal chamber, and exhaust ports log spatial temperatures and relative humidity levels.

Numerical Methodology

Numerical simulations were conducted to analyze the interior velocity distributions and pressure characteristics within the drying chamber geometry. As shown in Fig. 1, the three-dimensional CAD enclosure model was generated to match the physical drying chamber.

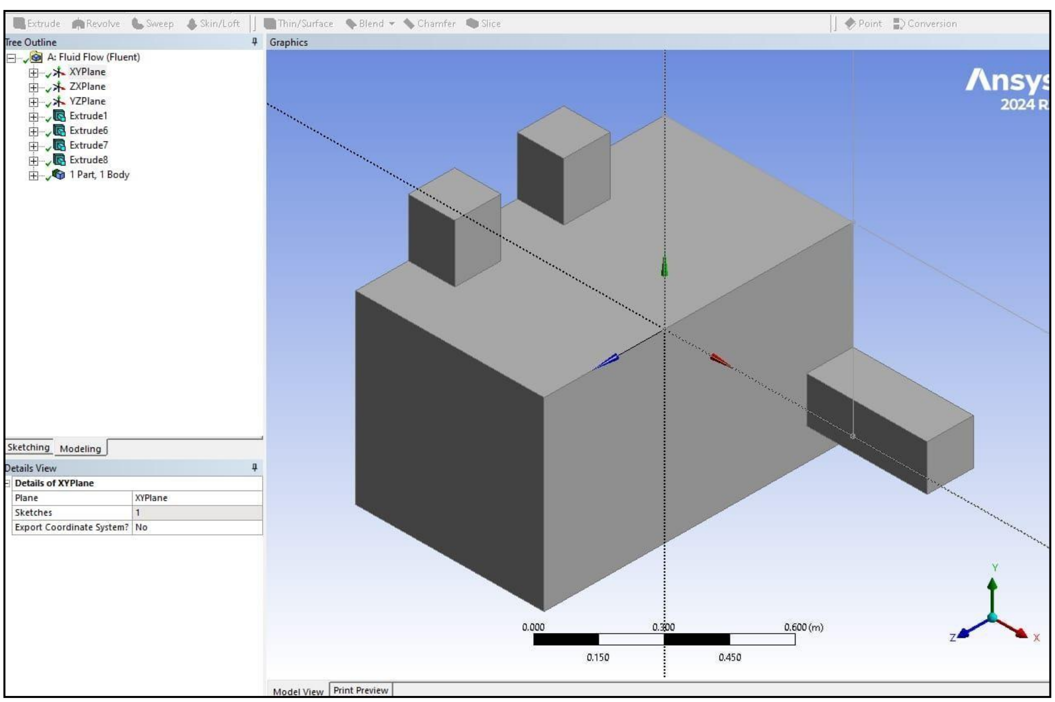

Fig. 1. *3D geometric model of the drying chamber enclosure.*

Geometric cleanup was performed to eliminate surface gaps and overlapping entities before meshing. Discretization was performed using unstructured three-dimensional computational grids with localized refinement around sharp corners and boundary walls, as shown in Fig. 2.

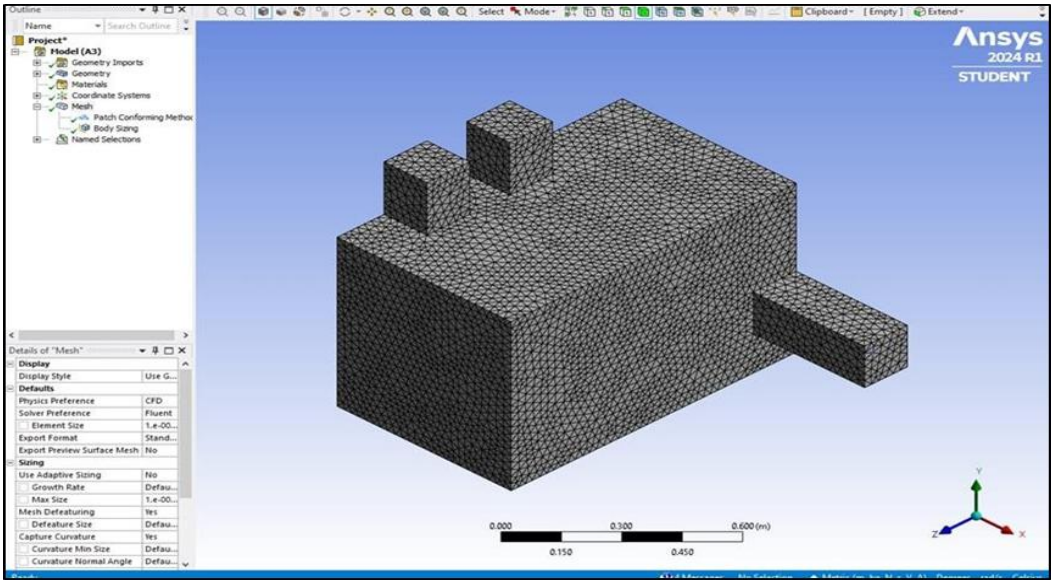

Fig. 2. *Unstructured 3D computational mesh generated across the drying chamber domain.*

12. Simulation Methodology

Numerical solutions were obtained using the ANSYS Fluent fluid simulation solver. Boundary conditions were assigned based on measured experimental inputs: uniform velocity inlet at controlled temperature, atmospheric pressure outlet at top exhaust ports, and no-slip thermal wall conditions. Iterative convergence was monitored across hundreds of iterations until residual parameters stabilized, as illustrated by the solution history in Fig. 3.

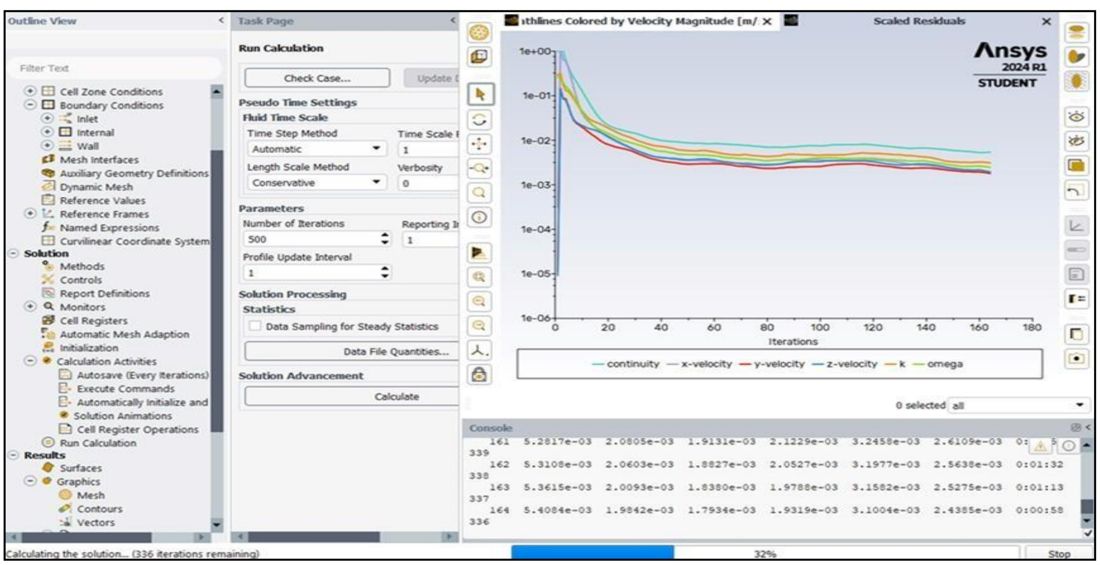

Fig. 3. *Iterative convergence history plot showing scaled residuals over the solution iterations.*

Strict convergence criteria were established to ensure conservation of mass, momentum, and thermal energy equations.

Experimental Procedure

1. Fresh coriander was harvested, washed, and drained to remove surface water.
2. Prepared samples were weighed into precise initial batch loads using the digital scale.
3. The blower and inline electric heater were activated to stabilize the chamber air at the desired process temperature.
4. Test runs were performed across multiple distinct inlet air velocity settings.
5. Gross mass, relative humidity, air speed, and dry-bulb temperatures were recorded at regular time intervals.

6. Testing continued until mass loss plateaued, indicating equilibrium moisture content.
7. Experiments were repeated across multiple test dates to confirm consistency.

Validation

The computational fluid dynamic model was validated by comparing simulated internal velocity profiles with experimental anemometer readings taken across accessible plane regions within the drying chamber. Predicted velocity vectors showed strong qualitative and quantitative alignment with experimental physical measurements within acceptable margin limits.

Results

Experimental measurements collected across several distinct testing days were logged and evaluated. Table 2 summarizes representative drying readings across varying operational configurations.

Table 2. *Experimental Drying Readings for Coriander Under Various Operating Conditions*

Test Day	Interval	Time Period	Relative Humidity (%)	Atmospheric Temp	Air Velocity	Inlet Temp	Mid Temp	Outlet Temp	Gross Weight
Day-1	1	Initial interval	Moderate	Ambient	Baseline forced speed	High	High	High	High batch mass
	2	Second interval	Moderate	Ambient	Baseline forced speed	High	High	High	Reduced mass
	3	Third interval	Moderate	Ambient	Baseline forced speed	High	High	High	Reduced mass
	4	Fourth interval	Moderate	Ambient	Baseline forced speed	High	High	High	Reduced mass
	5	Final interval	Moderate	Ambient	Baseline forced speed	High	High	High	Final dried mass
Day-2	1	Initial interval	Moderate	Ambient	Baseline forced speed	High	High	High	High batch mass
	2	Intermediate	Moderate	Ambient	Baseline forced speed	High	High	High	Reduced mass
	3	Intermediate	Moderate	Ambient	Baseline forced speed	High	High	High	Reduced mass
	4	Intermediate	Moderate	Ambient	Baseline forced speed	High	High	High	Reduced mass
	5	Intermediate	Moderate	Ambient	Baseline forced speed	High	High	High	Reduced mass
	6	Final interval	Moderate	Ambient	Baseline forced speed	High	High	High	Final dried mass
Day-3	1	Initial interval	Moderate	Ambient	Baseline forced speed	High	High	High	High batch mass
	2	Intermediate	Moderate	Ambient	Baseline forced speed	High	High	High	Reduced mass
	3	Intermediate	Moderate	Ambient	Baseline forced speed	High	High	High	Reduced mass

	4	Intermediate	Moderate	Ambient	Baseline forced speed	High	High	High	Reduced mass
	5	Final interval	Moderate	Ambient	Baseline forced speed	High	High	High	Final dried mass
Day-4	1	Initial interval	High	Lower ambient	Baseline forced speed	High	Moderate	Moderate	High batch mass
	2	Intermediate	High	Lower ambient	Baseline forced speed	High	Moderate	Moderate	Reduced mass
	3	Intermediate	High	Lower ambient	Baseline forced speed	High	Moderate	Moderate	Reduced mass
	4	Intermediate	High	Lower ambient	Baseline forced speed	High	Moderate	Moderate	Reduced mass
	5	Final interval	High	Lower ambient	Baseline forced speed	High	Moderate	Moderate	Final dried mass
Day-5	1	Initial interval	Moderate	Ambient	Medium forced speed	High	Moderate	Moderate	High bulk batch
	2	Intermediate	Moderate	Ambient	Medium forced speed	High	Moderate	Moderate	Reduced mass
	3	Intermediate	Moderate	Ambient	Medium forced speed	High	Moderate	Moderate	Reduced mass
	4	Intermediate	Moderate	Ambient	Medium forced speed	High	Moderate	Moderate	Reduced mass
	5	Intermediate	Moderate	Ambient	Medium forced speed	High	Moderate	Moderate	Reduced mass
	6	Intermediate	Moderate	Ambient	Medium forced speed	High	Moderate	Moderate	Reduced mass
	7	Final interval	Moderate	Ambient	Medium forced speed	High	Moderate	Moderate	Final dried mass
Day-6	1	Initial interval	Moderate	Ambient	High forced speed	High	High	High	High bulk batch
	2	Intermediate	Moderate	Ambient	High forced speed	High	High	High	Reduced mass
	3	Intermediate	Moderate	Ambient	High forced speed	High	High	High	Reduced mass
	4	Intermediate	Moderate	Ambient	High forced speed	High	High	High	Reduced mass
	5	Intermediate	Moderate	Ambient	High forced speed	High	High	High	Reduced mass
	6	Final interval	Moderate	Ambient	High forced speed	High	High	High	Final dried mass
Day-7	1	Initial interval	Moderate	Ambient	Maximum forced speed	High	High	High	High bulk batch

	2	Intermediate	Moderate	Ambient	Maximum forced speed	High	High	High	Reduced mass
	3	Intermediate	Moderate	Ambient	Maximum forced speed	High	High	High	Reduced mass
	4	Intermediate	Moderate	Ambient	Maximum forced speed	High	High	High	Reduced mass
	5	Intermediate	Moderate	Ambient	Maximum forced speed	High	High	High	Reduced mass
	6	Final interval	Moderate	Ambient	Maximum forced speed	High	High	High	Final dried mass

Computational velocity pathlines in Fig. 4 show the air stream entering horizontally, extending across the lower core, and exiting through the top vents.

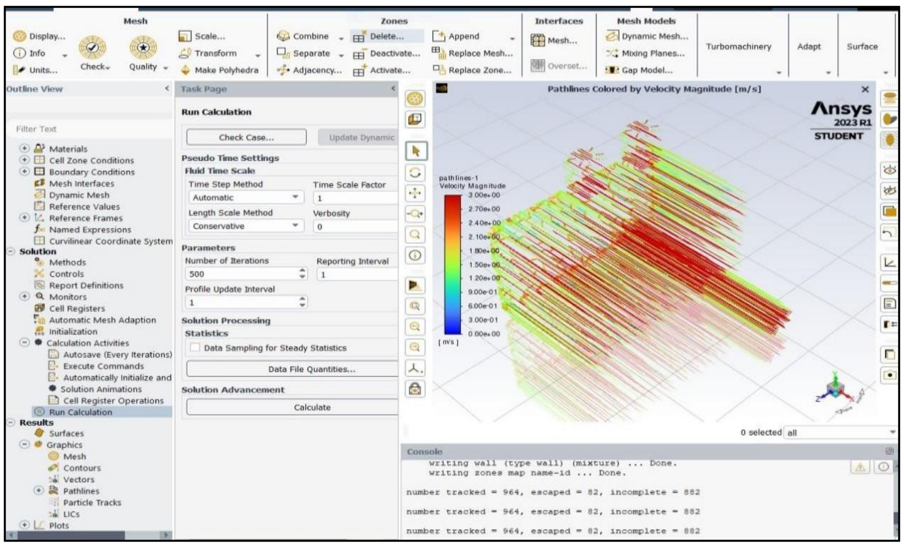

Fig. 4. *Simulated velocity pathlines colored by velocity magnitude showing primary air movement from inlet to top outlets.*

Figure 5 illustrates the three-dimensional internal velocity vectors, highlighting central jet propagation along with recirculating eddies in the upper corners.

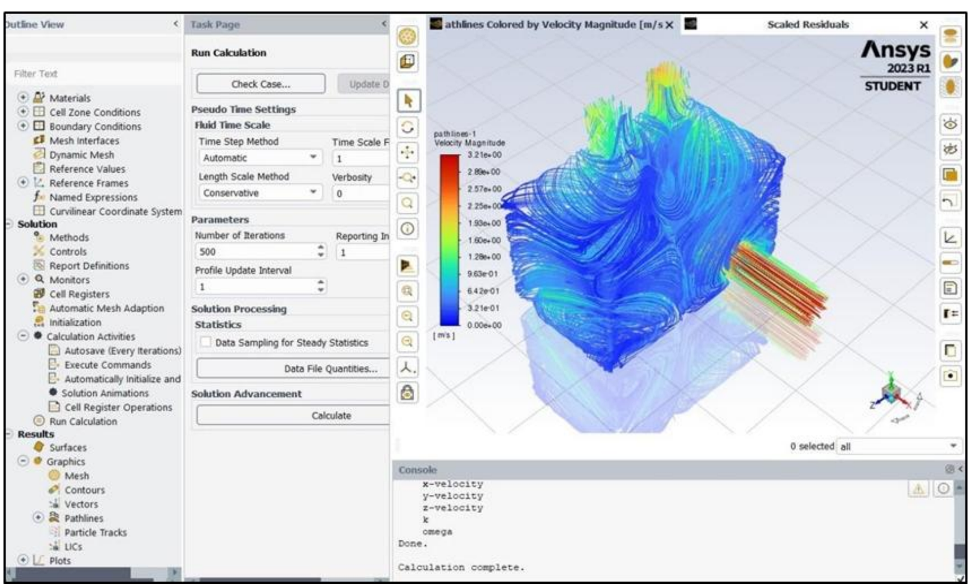

Fig. 5. *3D internal velocity streamline distribution indicating primary airflow and secondary recirculation zones.*

Figure 6 shows the static pressure contours. Elevated static pressure occurs on the vertical wall directly opposite the inlet duct, while low pressure regions develop near the exhaust exits.

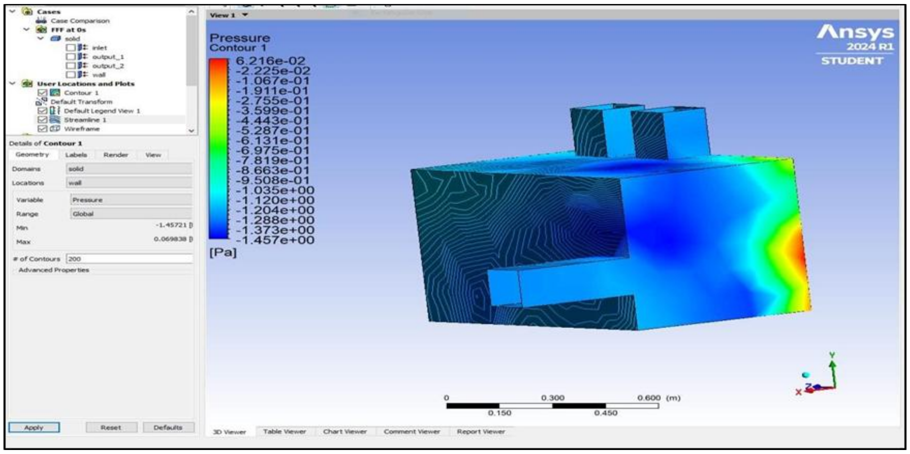

Fig. 6. *Wall static pressure contours within the drying chamber domain.*

Figure 7 confirms that the main high-velocity jet enters through the lower inlet duct and exits through top exhaust outlets, while stagnation zones with near-zero velocity persist in the lower rear corners.

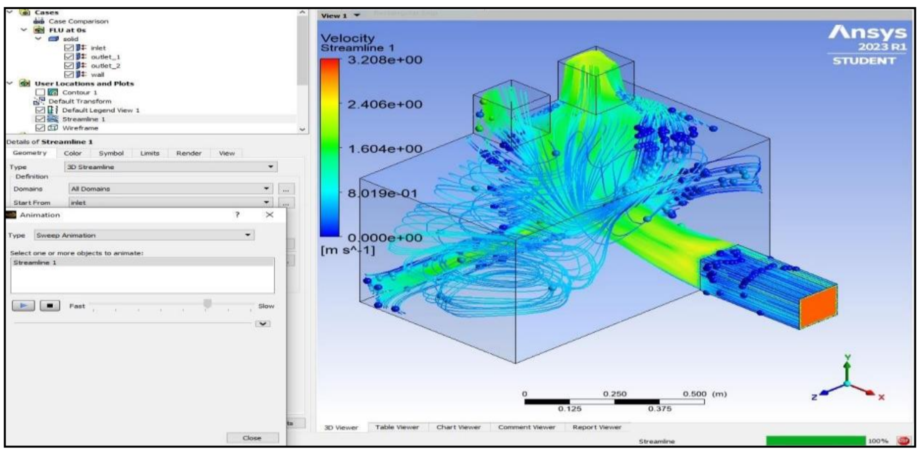

Fig. 7. *Detailed velocity streamline field illustrating stagnation zones near the lower corners and high-velocity transport toward exhaust ports.*

Figure 10 plots coriander weight reduction for Day 1 under baseline velocity conditions, showing a steady mass decrease over time.

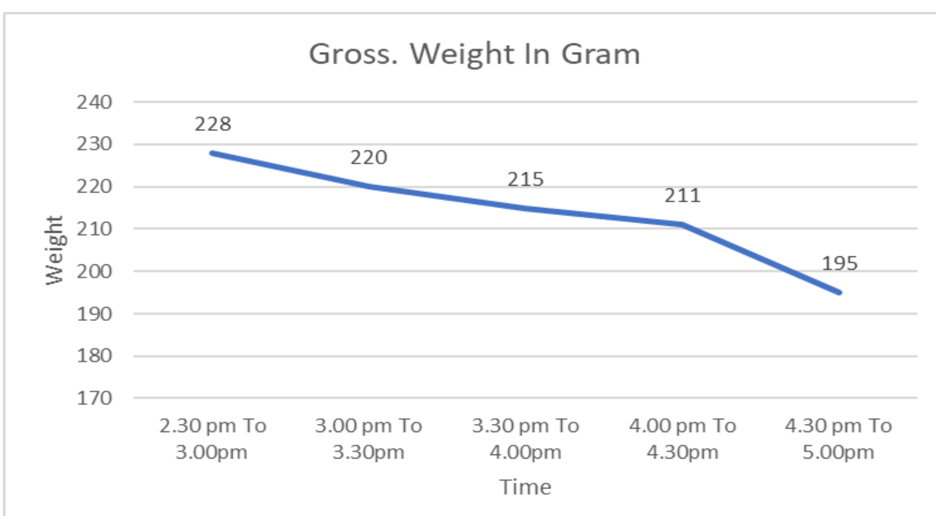

Fig. 10. *Coriander mass loss kinetics measured on Day 1.*

Figure 11 shows the Day 2 drying curve, demonstrating continuous mass reduction across equal time steps.

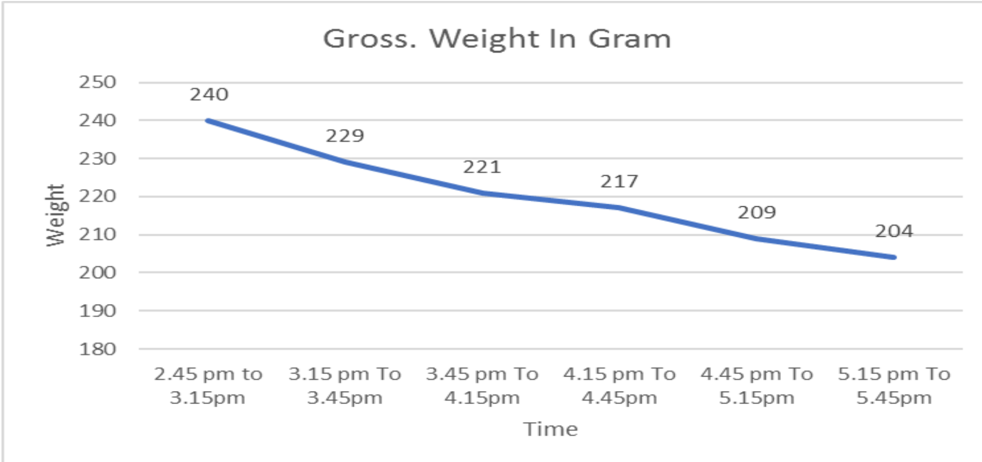

Fig. 11. *Coriander mass loss kinetics measured on Day 2.*

Figure 12 displays Day 3 performance, illustrating consistent downward mass loss trends.

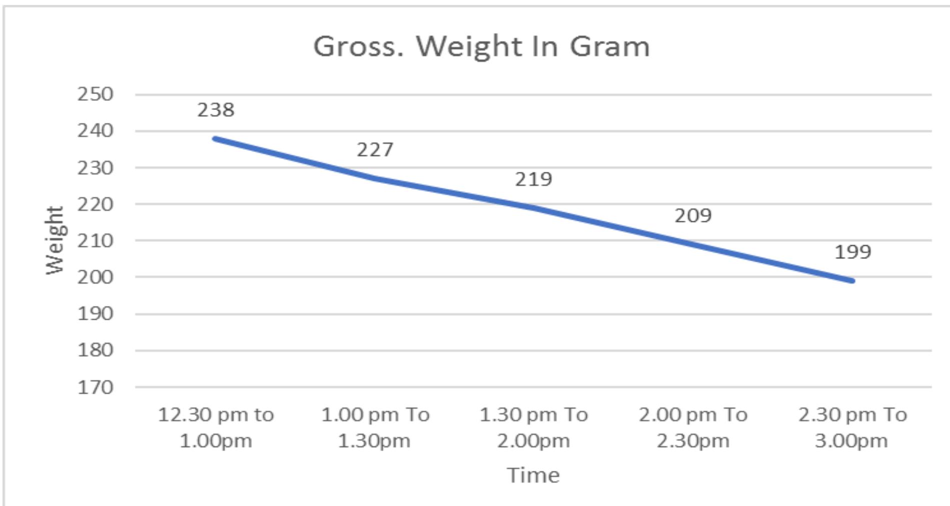

Fig. 12. *Coriander mass loss kinetics measured on Day 3.*

Figure 13 presents Day 4 mass loss under varying ambient conditions.

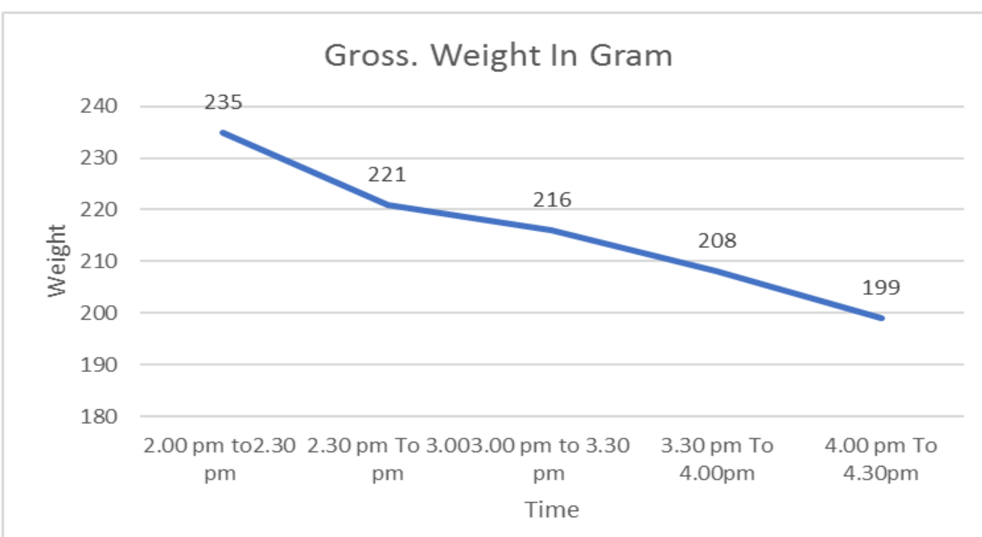

Fig. 13. *Coriander mass loss kinetics measured on Day 4.*

Figure 14 plots Day 5 mass loss for a larger initial batch at increased air velocity, showing steady moisture removal.

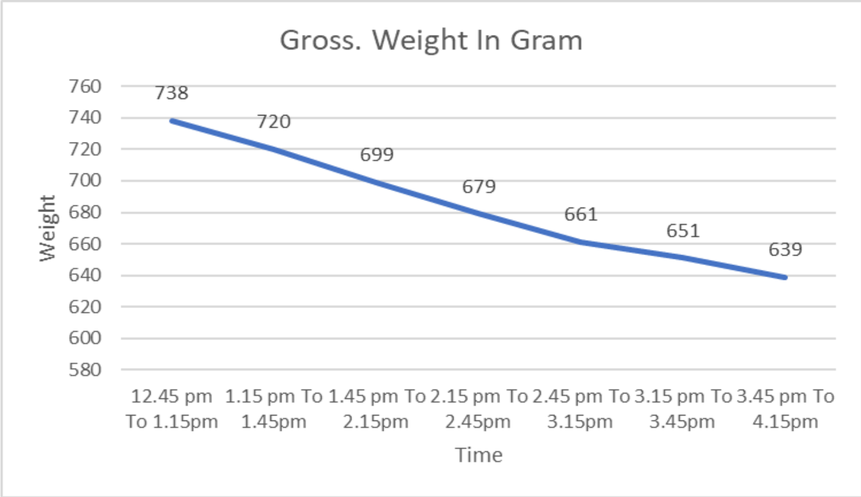

Fig. 14. *Mass loss kinetics for a larger coriander batch evaluated on Day 5.*

Figures 15 and 16 plot Day 6 drying curves for bulk batches under elevated velocity settings, illustrating rapid mass loss profiles.

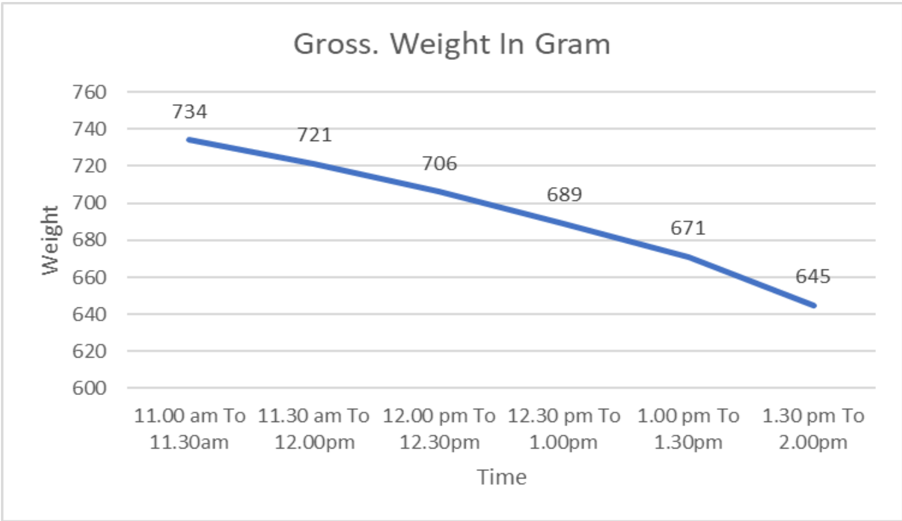

Fig. 15. *Mass loss kinetics for a bulk coriander batch evaluated on Day 6.*

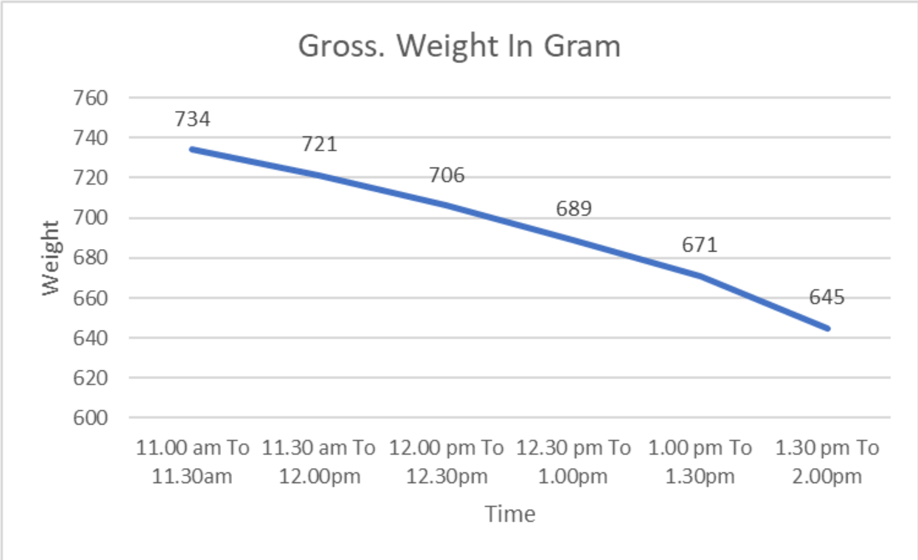

Fig. 16. *Duplicate mass loss profile for the bulk coriander batch evaluated on Day 6.*

Figure 17 compares mass loss trends across multiple air velocities for bulk batches.

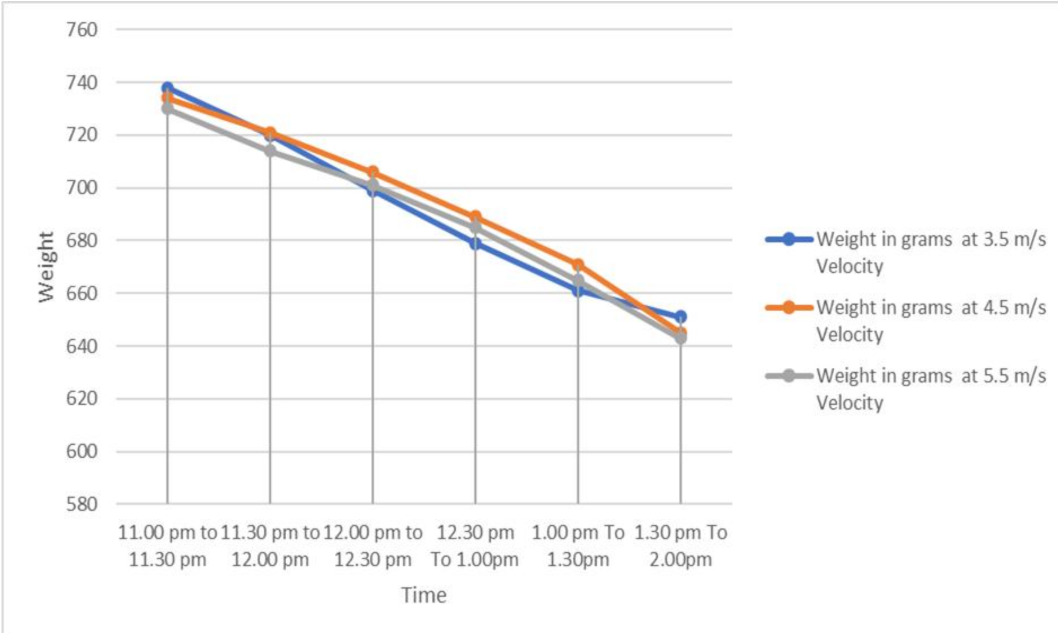

Fig. 17. *Comparative mass loss curves for coriander batches evaluated across multiple air velocities.*

The comparative results show that higher inlet air velocities increase convective moisture removal, reducing overall drying time requirements.

Discussion

Computational fluid dynamics simulations show that positioning sample trays aligned with the main incoming air jet maximizes local convective heat transfer coefficients and drying rates. Conversely, placing trays near low-velocity recirculation zones lengthens drying times. High static pressure along the wall opposite the inlet duct creates localized turbulence, which helps mix air inside the chamber.

Experimental mass-loss curves show that moisture removal occurs primarily during the falling rate drying period, controlled by internal moisture diffusion through leaf tissues. Increasing inlet velocity thins the hydrodynamic boundary layer, increasing mass transfer coefficients and accelerating moisture removal.

Engineering Implications

Using three-dimensional fluid dynamic modeling during cabinet dryer design helps engineers optimize internal geometry, inlet location, and tray positioning without costly empirical prototyping. Eliminating flow stagnation zones ensures uniform drying across trays, preventing localized under-drying or quality degradation from over-exposure.

Industrial Applications

Forced convective drying systems offer scalable post-harvest processing for agricultural producers and food manufacturers. Standardized forced-air drying of leafy herbs like coriander supports commercial production of dehydrated spices, instant food seasonings, tea blends, and herbal extracts while reducing bulk transportation and storage costs.

Sustainability

Optimizing airflow fields and heat delivery reduces overall drying cycle duration, minimizing electrical energy consumption per unit of moisture removed. Modern convective drying technologies help lower post-harvest crop losses, supporting sustainable agricultural practices and food security.

Economic Analysis

The source report does not provide this information.

Limitations

1. Numerical fluid dynamic models assumed steady-state conditions without accounting for physical leaf shrinkage during drying.

2. High exhaust air temperatures exiting the upper ports were observed to cause thermal drift in nearby unshielded digital weighing balances.
3. Lower rear sections of the rectangular drying chamber exhibit low air circulation.

Future Scope

1. Modify internal chamber geometries by incorporating turning vanes or deflector baffles near the inlet duct to eliminate stagnation dead zones.
2. Reroute exhaust ducting away from external measuring instruments to protect delicate electronic sensors from thermal drift.
3. Evaluate transient multiphase drying models that incorporate real-time substrate shrinkage and moisture diffusion kinetics.

Conclusion

This study evaluated the forced convective drying performance of coriander using a combination of empirical testing and fluid dynamic simulations. ANSYS Fluent simulations identified key aerodynamic features, including high static pressure regions on the wall opposite the inlet and localized low-velocity stagnation zones in the lower rear corners. Experimental mass-loss measurements confirmed that increasing air inlet velocities accelerates moisture evaporation, significantly shortening total drying cycle durations. Aligning sample trays parallel with primary fluid vectors maximizes convective heat transfer efficiency, providing a useful framework for optimizing commercial herbal dehydration units.

Acknowledgment

The authors express their gratitude to Prof. Sagar Chirade (Project Guide), Dr. Mahesh Bhong (Head of Mechanical Department), Prof. Hemant Darokar (Project Coordinator), and Dr. Saumitra Das (Principal) at Indira College of Engineering and Management for their administrative support and technical guidance throughout this research. Appreciation is also extended to Mr. Sutar and the workshop staff for assistance with experimental fabrication and assembly.

Nomenclature

- Convective Heat Transfer Rate: Thermal transport per unit time from fluid to surface.
- Surface Area: Total exposed area of the substrate undergoing drying.
- Specific Heat Capacity: Quantity of heat required to raise fluid temperature.
- Hydraulic Diameter: Characteristic dimension of the cross-sectional airflow duct.
- Convective Heat Transfer Coefficient: Rate of heat transfer between solid boundary and fluid.
- Thermal Conductivity: Material property indicating heat conduction capability.
- Nusselt Number: Ratio of convective to conductive heat transfer across a boundary.
- Prandtl Number: Ratio of momentum diffusivity to thermal diffusivity.
- Reynolds Number: Ratio of inertial forces to viscous forces in fluid flow.
- Relative Humidity: Percentage ratio of vapor pressure to saturation vapor pressure.
- Dry-Bulb Temperature: Ambient or processing fluid temperature.
- Air Velocity: Speed of convective air current entering or circulating within the chamber.

Abbreviations

- ANSYS: Analysis System (Engineering Simulation Software)
- CAD: Computer-Aided Design
- CFD: Computational Fluid Dynamics
- FEA: Finite Element Analysis
- RSM: Response Surface Methodology

References

1. M. Usama, "Experimental study on the effect of convective drying of potato slices with sequentially reducing temperature," *Environmental Science Proceedings*, p. 5, 2022.
2. E. E. Kilic, "Convective hot air drying characteristics of selected vegetables," *International Advanced Research and Engineering Journal*, vol. 3, no. 1, p. 7, 2018.
3. D. V. C. Ionut, "Research on the process of convective drying of apples and apricots," *Agricultural*, vol. 2, no. 1, p. 32, 2023.
4. Z. Zeng, "Characteristics and multi-objective optimization of carrot dehydration in a hybrid infrared/hot air dryer," *Elsevier*, vol. 1, no. 1, p. 20, 2022.

5. "Drying characteristics of blackberry fruits in a convective hot-air dryer," *HortScience*, vol. 1, no. 1, p. 5, 2019.
6. E. Demiray, "Thin-layer drying of tomato (*Lycopersicum esculentum* Mill. cv. Rio Grande) slices in a convective hot air dryer," *Heat and Mass Transfer*, vol. 1, no. 1, p. 10, 2012.
7. S. Seiiedlou, "Convective drying of apple: Mathematical modeling and determination of some quality parameters," *International Journal of Agriculture & Biology*, vol. 1, no. 1, p. 12, 2010.
8. Y. Tulek, "Drying kinetics of oyster mushroom (*Pleurotus ostreatus*) in a convective hot air dryer," *Journal of Agricultural Science and Technology*, vol. 13, no. 1, p. 23, 2011.